Available online at www.sciencedirect.com
ScienceDirect
Journal of Hazardous Materials 149 (2007) 725–734
Journal of Hazardous Materials
www.elsevier.com/locate/jhazmat

Photocatalytic degradation of Azure and Sudan dyes using nano TiO_2

T. Aarthi, Prashanthi Narahari, Giridhar Madras *

Department of Chemical Engineering, Indian Institute of Science, Bangalore 560012, India

Received 14 October 2006; received in revised form 11 December 2006; accepted 15 April 2007
Available online 20 April 2007

Abstract

The present study investigates the dependence of photocatalytic rate on molecular structure of the substrate that is degraded. The photocatalytic degradation of Azure (A and B) and Sudan (III and IV) dyes, having similar structure, but different functional groups, were investigated with two catalysts. The photocatalytic activity of solution combustion synthesized TiO_2 (CS TiO_2) was compared with that of Degussa P-25 for degrading these dyes. The effect of solvents and mixed-solvent system on photodegradation of Sudan III was investigated. The photodegradation rate was found to be higher in solvents with higher polarity. The effect of pH and the presence of metal ions in the form of chloride and nitrate salt, on degradation rate of Azure A was also investigated. The metal ions significantly reduced the photocatalysis rates. A detailed Langmuir–Hinshelwood kinetic model has been developed to explain the effect of metal ions on degradation rate of the substrate. This model elucidates the contribution of holes and electrons towards degradation of the dye.

Keywords: Photocatalysis; Azure; Sudan; TiO_2; Dye degradation; Combustion synthesis

1. Introduction

Photocatalysis is a process by which a semiconducting material absorbs light of energy more than or equal to its band gap, thereby generating holes and electrons, which can further generate free-radicals in the system to oxidize the substrate. The resulting free-radicals are very efficient oxidizers of organic matter. The degradation of organic compounds is the most widely used photocatalytic application of nanocrystalline TiO_2 [1–3]. A detailed analysis of electronic and charge–transfer processes occurring during heterogeneous photocatalysis on TiO_2 has been summarized in reviews [4,5]. The photocatalytic degradation of dyes by TiO_2 has been extensively and prominently explored in many previous studies [6,7]. The mode of synthesis of TiO_2 influences the photocatalytic activity of the catalyst (i.e., band gap, bounded hydroxyl species, crystallinity and particle size). The anatase phase nano titania (TiO_2) prepared by the solution combustion method has been reported to have better photocatalytic activity compared to the commercial Degussa P-25 catalyst [8,9].

The effect of molecular structure and functional groups on the photodegradation rate on substituted phenols [10], nitroaromatics [11], multi-substituted phenols [12], nitrogen moieties in surfactants [13] and number of azo groups in dyes [14] has been illustrated. The present study aims at determining the dependence of photocatalysis of dye substrates with similar structures but different functional groups. Hence, a pair of Azure dyes and a pair of Sudan dyes was chosen for this study. Fig. 1 shows the structure of the dyes Azure A, Azure B, Sudan III and Sudan IV. The replacement of H by methyl group in Azure A gives the dye Azure B. The addition of two methyl groups, one to each benzene ring of Sudan III gives the dye Sudan IV. Azure dyes are soluble completely in water and sparingly in ethanol. Sudan dyes are insoluble in water but soluble in aromatic hydrocarbons (like toluene, xylene and high boiling aromatic blend) and ethanol. The effect of solvents on photodegradation has been investigated in earlier studies [15]. The effect of organic solvents on photodegradation of a dye soluble in organic solvents, but insoluble in water, could be interesting to investigate. Hence, the effect of solvents and mixed-solvent system on the photodegradation of Sudan III has been investigated in this work. Dye containing polluted water also contains metal ions. Several studies report the retardation effect of inorganic salts on the photodegradation of pollutants, like NaCl on phenol degradation [16], NaCl, Na_2SO_4, etc., on azo dyes [17],

* Corresponding author. Tel.: +91 80 309 2321; fax: +91 80 309 2321.
E-mail address: giridhar@chemeng.iisc.ernet.in (G. Madras).

0304-3894/$ – see front matter © 2007 Elsevier B.V. All rights reserved.
doi:10.1016/j.jhazmat.2007.04.038

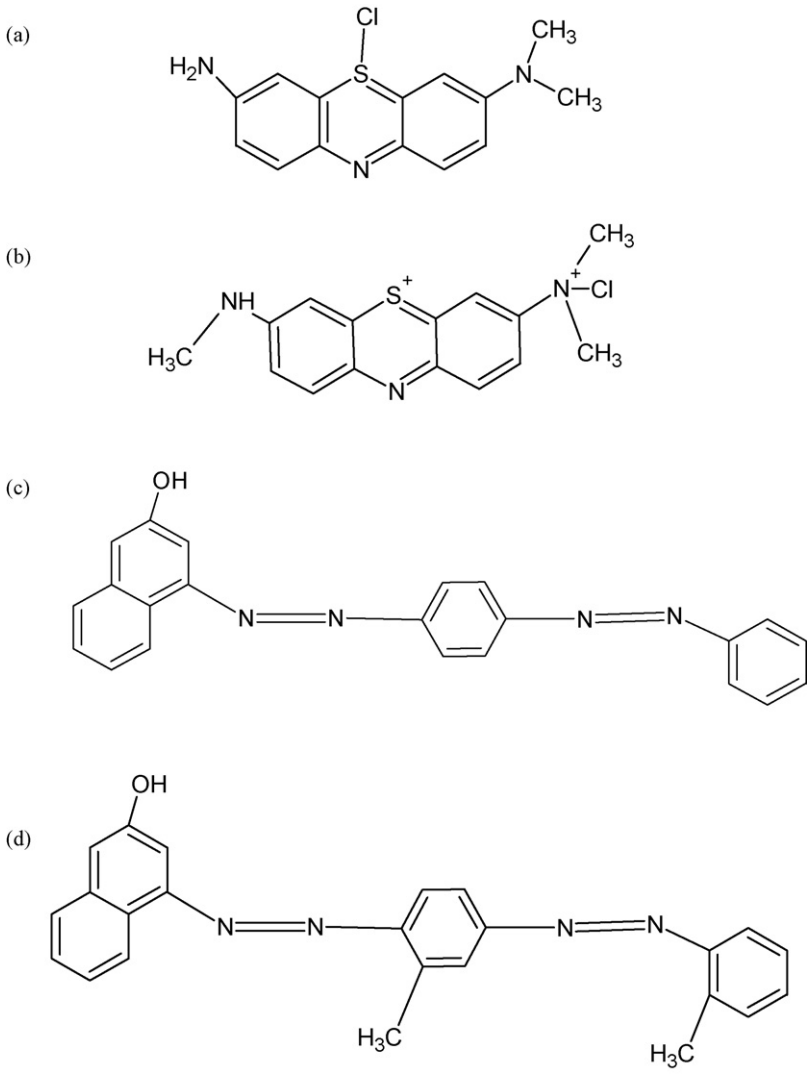

Fig. 1. Structure of (a) Azure A; (b) Azure B; (c) Sudan III and (d) Sudan IV.

transition metal ions such as Cu^{2+} and Fe^{3+} on several dyes [18]. Therefore, the effect of metal ions like Cu^{2+}, Zn^{2+}, Al^{3+}, Co^{2+} on the degradation rate of Azure A has been investigated. To study the effect of anion, the presence of chloride and nitrate salts were investigated. To model the retardation kinetics, experiments were conducted at different concentration of copper salt and a detailed Langmuir–Hinshelwood kinetics was developed. The effect of pH on photocatalysis has been extensively studied and a review on this aspect can be found elsewhere [3]. In this study, the effect of pH on photocatalysis by combustion synthesized TiO_2 has also been investigated.

The objective of the work is to determine the effect of functional groups on the degradation rates of water-soluble and water insoluble dyes in the presence of the combustion synthesized catalyst for the first time. The effect of metal ions and solvents on the degradation of the dyes has also been investigated and a new detailed Langmuir–Hinshelwood kinetic model has been developed for the first time to explain the effect of metal ions on degradation rate of the substrate and clearly differentiate the contribution of holes and electrons towards degradation of the dye.

2. Experimental

2.1. Materials

The dyes, Azure A (AA, $C_{14}H_{14}ClN_3S$, CAS: 531-53-3) and Azure B (AB, $C_{15}H_{16}ClN_3S$, CAS: 531-55-5) were purchased from S.D. Fine Chemicals (India). Sudan III (S3, $C_{27}H_{16}N_4O$, CAS: 85–86-9) and Sudan IV (S4, $C_{24}H_{20}N_4O$, CAS: 85–83-6) were purchased from Rolex Industries (India). Titanium isopropoxide (Lancaster Chemicals, UK), and glycine (Merck, India) were used in the preparation of catalyst. The salts, cupric nitrate, cobalt nitrate, aluminium nitrate, zinc nitrate, ferric chloride, cobalt chloride, copper chloride and nitric acid were purchased from S.D. Fine Chemicals (India). Double-distilled water was filtered through a Millipore membrane filter before use.

2.2. Catalyst preparation

The solution combustion method [9,10] was used to prepare nano-sized anatase TiO_2. The precusor titanyl nitrate [$TiO(NO_3)_2$] and the fuel glycine ($H_2N–CH_2–COOH$) were used in this method. Titanyl hydroxide [$TiO(OH)_2$] was obtained by the hydrolysis of titanium isopropoxide [Ti(*i*-OPr)$_4$] and reacted with nitric acid to yield Titanyl nitrate. In a typical combustion synthesis, a Pyrex dish (with a volume of 300 cm^3) containing an aqueous redox mixture of stoichiometric amounts of titanyl nitrate and glycine in 30 mL water was introduced into a muffle furnace that was preheated at 350 °C. The solution initially undergoes dehydration and a spark appears at one corner, which spreads throughout the mass, finally yielding anatase titania. Thus, TiO_2 was formed by the complete combustion of the titanyl-glycine redox mixture. The liberation of the large volumes of the gases leads to the high porosity and high surface area of the material.

2.3. Catalyst characterization

The catalyst has been characterized by various techniques such as XRD, TEM, BET, TG-DTA, XPS, IR, UV spectroscopy [8,9]. The X-ray diffraction (XRD) patterns of catalysts were recorded on a Siemens D-5005 diffractometer using Cu Kα radiation with a scan rate of 2° min^{-1}. The XRD pattern of combustion synthesized TiO_2 was recorded in 2θ range from 5 to 100°. The pattern can be indexed to pure anatase phase of TiO_2 with the space group of *I*41/*amd*. The data were then refined using Fullprof-98 program. There was a good agreement between calculated and observed pattern. The lattice parameter for TiO_2 is $a = 3.7865$ (5) Å and $c = 9.5091$ (1) Å. The crystallite size was determined from XRD pattern using Sherrer formula and based on the full width half maxima (FWHM) of X-ray diffraction pattern, the mean crystallite size is estimated to be 10 ± 2 nm. Transmission electron microscopy (TEM) of powders was carried out using a JEOL JEM-200CX transmission electron microscopy operated at 200 kV. TEM studies also showed the crystallites of TiO_2 are homogeneous with the mean size of 8 ± 2 nm, which agrees well with the XRD measurements. The surface area of the catalyst was determined with standard BET apparatus (NOVA-1000, Quantachrome) and was 240 $m^2\,g^{-1}$ and is higher than the surface area of commercial catalysts like Degussa P-25 (50 $m^2\,g^{-1}$). Fourier transform infrared (FTIR) studies were carried out in the 400–4000 cm^{-1} frequency range in the transmission mode (Perkin–Elmer, FTIR-Spectrum-1000) and showed higher surface hydroxyl content for the combustion synthesized TiO_2. The synthesized TiO_2 was subjected to thermogravimetric-differential thermal analysis (TG-DTA) (Perkin–Elmer, Pyris Diamond), which showed a 11% weight loss indicating more surface hydroxyl groups. X-ray photoelectron spectra (XPS) of these materials were recorded with ESCA-3 Mark II spectrometer (VG Scientific Ltd. England) using Al Kα radiation (1486.6 eV). UV–vis absorption spectra of TiO_2 powders were obtained for the dry pressed disk samples using UV–vis spectrophotometer (GBC Cintra 40, Australia) between 270 and 800 nm range. The combustion synthesized TiO_2 shows two optical absorption thresholds at 570 and 467 nm that corresponds to the band gap energy of 2.18 and 2.65 eV, respectively. Further details on catalyst preparation and characterization are provided elsewhere [8,9].

2.4. Photochemical reactor

The photochemical reactor employed in this study was comprised of a jacketed quartz tube of 3.4 cm I.D., 4 cm O.D., and 21 cm length and an outer Pyrex glass reactor of 5.7 cm I.D. and 16 cm length. The UV light was provided by a 125 W high pressure mercury vapor lamp (Philips, India) was used after removal of the outer shell and placed inside the jacketed quartz tube. The ballast and capacitor were connected in series with the lamp to avoid fluctuations in the input supply. Water was circulated through the annulus of the quartz tube to avoid heating of the solution due to dissipative loss of UV energy. The solution was taken in the outer reactor and continuously stirred using a magnetic stirrer to ensure that the suspension of the catalyst was uniform during the course of the reaction. Further details of the experimental set-up can be found elsewhere [8].

2.5. Degradation experiments

During the degradation of each of the dyes, a known mass of the dye was dissolved in Millipore-filtered double-distilled water and subjected to UV irradiation in the photochemical reactor described above with a catalyst loading of 1 g L^{-1}. The reactions were carried out at 40 °C, which was maintained by circulating water in the annulus of the jacketed quartz reactor. Samples were collected at regular intervals, filtered through Millipore membrane filters, and centrifuged to remove the catalyst particles prior to analysis.

2.6. Sample analysis

The molar absorptivity of dyes employed is measurably high for even dilute solutions. Therefore, photometric studies were carried out for the dyes used. The UV–vis spectrophotometer (Shimazdu, UV 2100) with quartz cuvettes was used for the determination of color intensity in the range of 190–700 nm. The λ_{max} values of Azure A, Azure B, Sudan III and Sudan IV are 625, 650, 512 and 357 nm, respectively. The UV spectrum before and after degradation showed a decrease of peak corresponding to the dye but did not show any new peaks, indicating that no detectable intermediates were formed during the reaction. Calibration based on Beer–Lambert law was used to quantify the dye concentration.

3. Results and discussion

All the experiments were conducted at the natural pH of the dye with a catalyst concentration of 1 g L^{-1}. This catalyst concentration was determined by conducting the experiments at various catalyst concentrations. The reaction rate did not increase significantly after the catalyst concentration of 1 g L^{-1}, consistent with the results obtained for the degradation of other

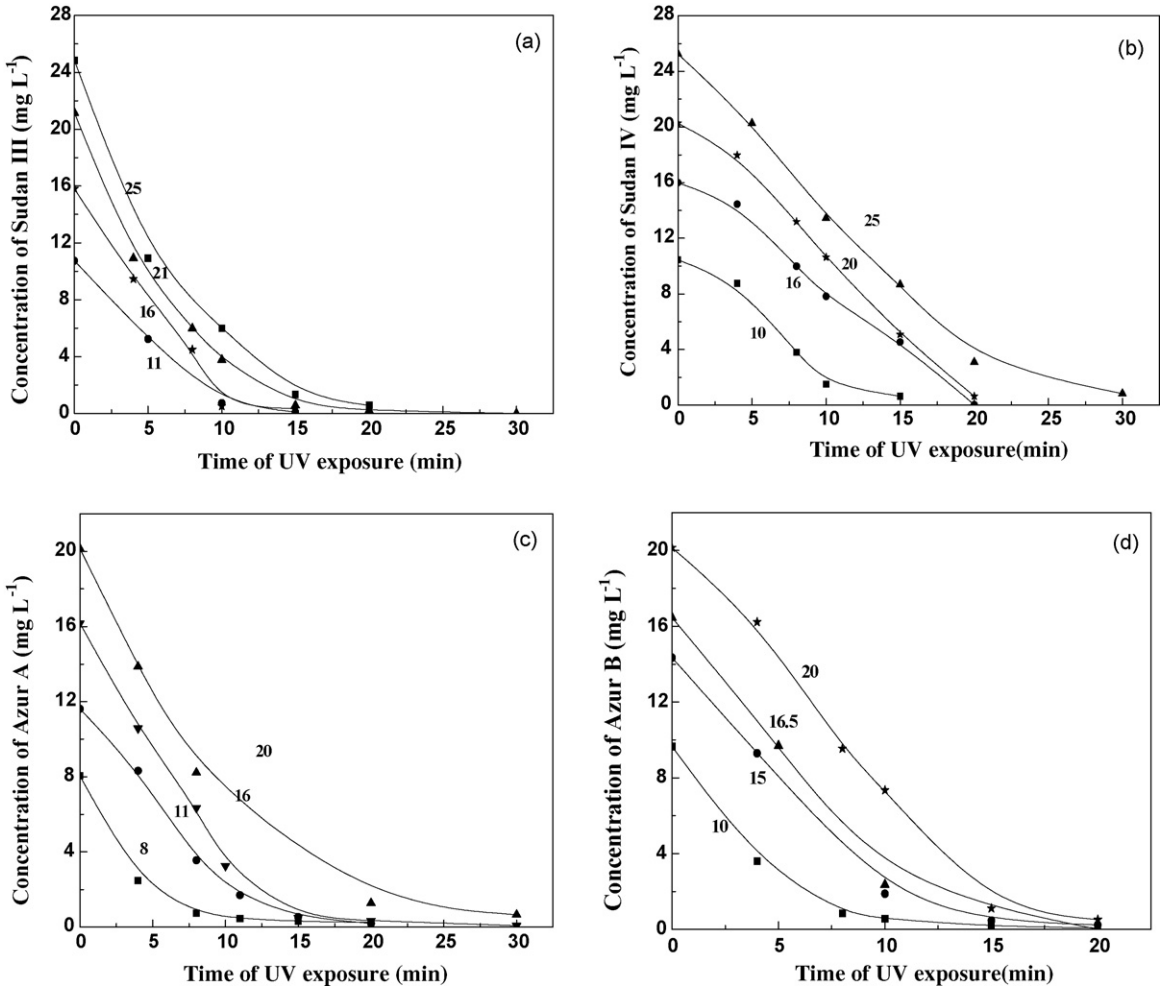

Fig. 2. Concentration profiles of (a) Sudan III; (b) Sudan IV; (c) Azure A and (d) Azure B dyes when degraded with 1 g L^{-1} CS TiO_2. The numbers on the figures denote the initial concentration of the dyes in mg L^{-1}.

dyes with the same catalyst [8]. After the addition of the catalyst, the dye solution was stirred for 30 min to ensure that the equilibrium adsorption/desorption of the dye on the catalyst was attained. The corresponding concentration of the dye (as measured by UV spectrophotometer and the concentration evaluated using Beer–Lambert's law) was taken as the initial concentration of the dye for all the catalyzed reactions. The solvent used for Azure and Sudan was water and ethanol, respectively. Fig. 2a–d shows the variation of concentration profile of various dyes, at different initial concentrations, in CS TiO_2 catalyzed system. The initial rates of the reaction were determined by extrapolating the tangent (based of the linear fit of the first four points) of the concentration profile back to initial conditions. The slopes calculated at the initial three to six points were nearly constant, indicating the accuracy of the initial rates reported in this study.

The model is developed by following the photocatalytic mechanism, which is well understood and reported [4–6,9]. The positive holes and electrons generated by UV on photocatalyst, involve in the formation of the hydroxyl radicals. The reaction between the positive holes and the adsorbed water forms hydroxyl species. There is a series of steps involved in the formation of $OH^{\bullet}$ by electron pathway. The dye degrades by the attack of direct hole and hydroxyl species. The presence of Cu^{2+} reduces the concentration of e^- because of reduction of Cu^{2+} to Cu^+ by e^-. Consequently, this scavenging reduces the formation of $OH^{\bullet}$ by the e^- pathway (though the formation of $OH^{\bullet}$ by hole pathway remains unaffected). The kinetic model reported in this work includes the generation of $OH^{\bullet}$ radicals via electron pathway for the photocatalytic degradation of dyes and it is an extension of the model reported in a previous study [9,19]. In this work, we have included this pathway and the scavenging of electrons by metal to derive the rate equation in terms of dye and the concentration of retardant Cu^{2+}. The mechanism and kinetics are discussed in detail in Appendix A.

By writing the stoichiometric balances for all the species using the mechanism and by applying the quasi-steady state assumption (QSSA) for all the intermediate species,

$$-r_D = k_{OH}[D] + k_1[D]\left(\frac{k_3}{1+K_2[D]} + \left(\frac{k_4}{1+K_2[D]}\right) \times \left(\frac{1}{1+K_6[C^{2+}]}\right)\right) \quad (1)$$

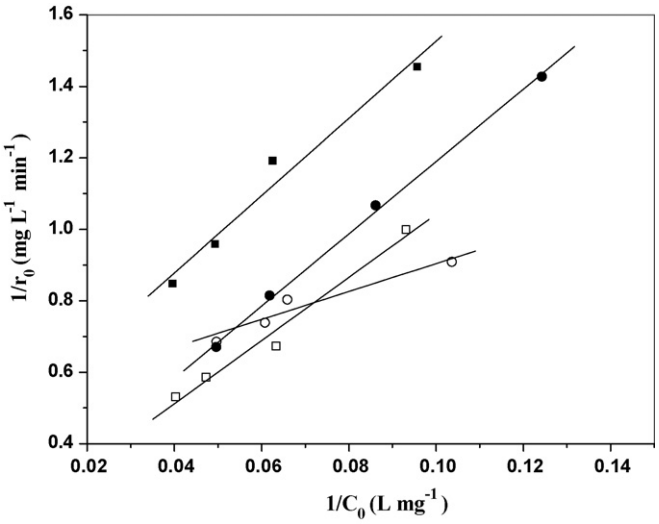

Fig. 3. Variation of the inverse of initial rate with the inverse of initial concentration of the dyes: □, Sudan III; ■, Sudan IV; ●, Azure A and ◯, Azure B.

Eq. (1) gives the relation between the photocatalytic degradation rate, r_D and the concentration of dye [D] and the concentration of the retardant metal $[C^{2+}]$ and indicates that the competitive adsorption of the metal lowers the rate of photocatalysis. The rate constants, k_1k_3 and k_1k_4 refer to the generation of $OH^\bullet$ by hole and electron pathway, respectively. Taking inverse of Eq. (1) and neglecting the quadratic term of [D], we get

$$\frac{1}{r_D} = \left(\frac{1}{[D]} + K_2\right) \frac{\{1 + K_6[C^{2+}]\}}{\{k_0 + K_6k_7[C^{2+}]\}} \quad (2)$$

where $k_0 = k_{OH} + k_1k_3 + k_1k_4$ and $k_7 = k_{OH} + k_1k_3$

When no metal ion is present, $[C^{2+}] = 0$, the variation of the inverse of the initial rate is given by

$$\frac{1}{r'_{D,0}} = \left(\frac{1}{[D]} + K_2\right) \frac{1}{k_0} \quad (3)$$

Experiments were conducted without catalyst in presence of UV. In this case, the rate of degradation is directly proportional to the dye concentration. The degradation rate constants of Sudan III and Sudan IV were nearly the same, whereas in case of Azure dyes, the rate constant of Azure B was 2.1 times higher than that of Azure A. In case of CS TiO_2 catalyzed system, the inverse of initial rates, $r_{D,0}$ varies linearly with the inverse of the initial concentration [D] as given by Eq. (3) for various dyes. This variation is shown in Fig. 3. The values of k_0 and K_2 were obtained from the linear regression and are tabulated in Table 1. Similar to the experiments without catalyst, in case of CS TiO_2 catalyzed system, there was no significant difference in k_0 value among Sudan dyes, in spite of two additional methyl groups in Sudan IV. This could be attributed to the primary step being the attack in the ring that is present in both these dyes. However, the adsorption coefficient of Sudan IV is nearly five times that of Sudan III. Whereas, in case of Azure dyes, degradation rate constant of Azure B was 1.5 times of that of Azure A and the adsorption coefficient of Azure B is more than twice that of Azure A, indicating that Azure B has more affinity on TiO_2 compared to that of Azure A. This confirms that the photocatalysis rate inherently depends on the structure of the substrate that has to be degraded.

Table 1
Rate constants for the photocatalytic degradation of dyes in the presence of CS TiO_2

Dye	System	k_0 (min^{-1})	K_2($L\,mg^{-1}$)
Sudan III	CS TiO_2	0.110	0.010
	No catalyst	0.014	–
Sudan IV	CS TiO_2	0.100	0.050
	No catalyst	0.012	–
Azure A	CS TiO_2	0.17	0.060
	No catalyst	0.004	–
Azure B	CS TiO_2	0.260	0.130
	No catalyst	0.009	–

Comparing the catalysts CS TiO_2 and Degussa P-25, at the constant initial concentration of the dyes, say 21 mg L^{-1}, in case of Sudan III, the initial rates were higher for CS TiO_2 compared to that of Degussa P-25, where the initial rate was 1 and 1.7 mg L^{-1} min^{-1} for Degussa P-25 and CS TiO_2, respectively. Similarly in case of Sudan IV, the initial rates were 0.7 and 2.1 mg L^{-1} min^{-1}, respectively, for Degussa P-25 and CS TiO_2. This could be attributed to the lower band gap value (2.18 and 2.6 eV for CS TiO_2, 3.1 eV for Degussa P-25 catalyst) [8,9], higher hydroxyl content (as shown by TG, IR studies done previously) and smaller size/higher surface area of CS TiO_2 compared to Degussa P-25 (240 m^2 g^{-1} for CS TiO_2, 50 m^2 g^{-1} for Degussa P-25). However, in case of Azure A, the initial degradation rates were 3 and 1.5 mg L^{-1} min^{-1} for Degussa P-25 and CS TiO_2, respectively. Similarly, in case of Azure B, the initial degradation rates were 2.4 and 1.3 mg L^{-1} min^{-1}, for Degussa P-25 and CS TiO_2, respectively (see Fig. 4).

The effect of solvents and mixed-solvent systems on photodegradation of dye Sudan III was also investigated. As the ethanol content in the system increased, the rate decreased. Fig. 5 shows the variation of the degradation rate with % ethanol in the system. This could be attributed to the scavenging of OH radicals by these solvents or solubility of electrons, which are essential for generating OH radicals. If latter is the reason, one can expect higher degradation in more polar solvents than in less polar solvents. The dielectric constants of methanol and ethanol are 32.6 and 24.3, respectively. Therefore the possibility to generate OH radical in protic solvent like methanol is much higher compared to that of ethanol and consequently increases the rate of the degradation.

When the concentration of the nitrate salt was 200 μM, the presence of metal ions like Cu^{2+}, Al^{3+}, Co^{2+} and Zn^{2+}, reduced the initial rates of photocatalytic degradation of Azure A in the presence of CS TiO_2, by 72, 53, 64 and 62%, respectively, as shown in Fig. 6a. When the concentration of chloride salt was 200 μM, the presence of Cu^{2+}, Co^{2+}, Fe^{3+}, reduced the initial rates of photocatalytic degradation of Azure A by 88, 68 and 42%, respectively, as shown in Fig. 6b. In a previous study [18], it was shown that the presence of metal ions (added as nitrate salt), $Cu^{2+}$and Zn^{2+} reduced the rates for the degradation of malachite green by 76 and 66%, respectively. It is known that

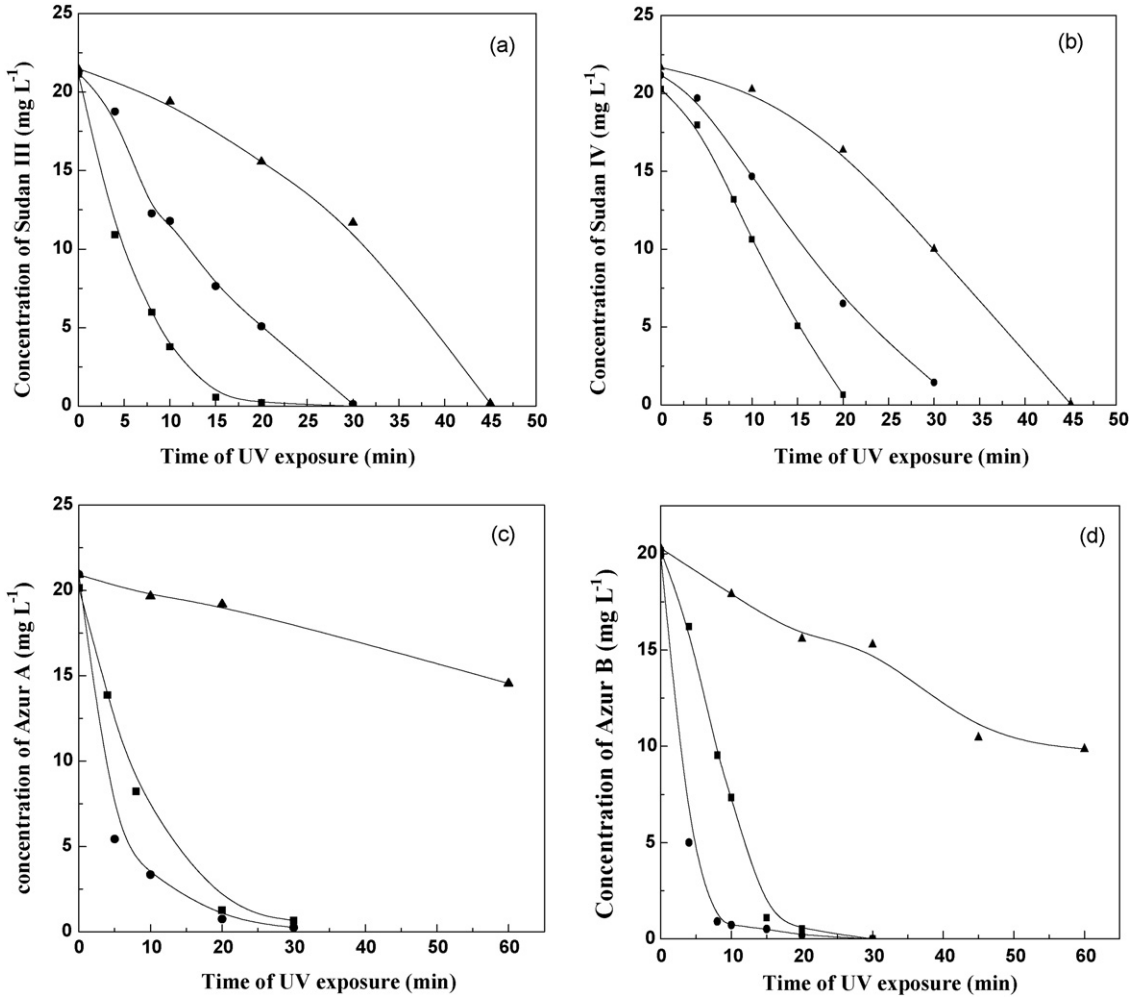

Fig. 4. Effect of catalyst on the photocatalytic degradation of (a) Sudan III; (b) Sudan IV; (c) Azure A and (d) Azure B with □, CST; ●, Degussa P-25 and ▲, without catalyst.

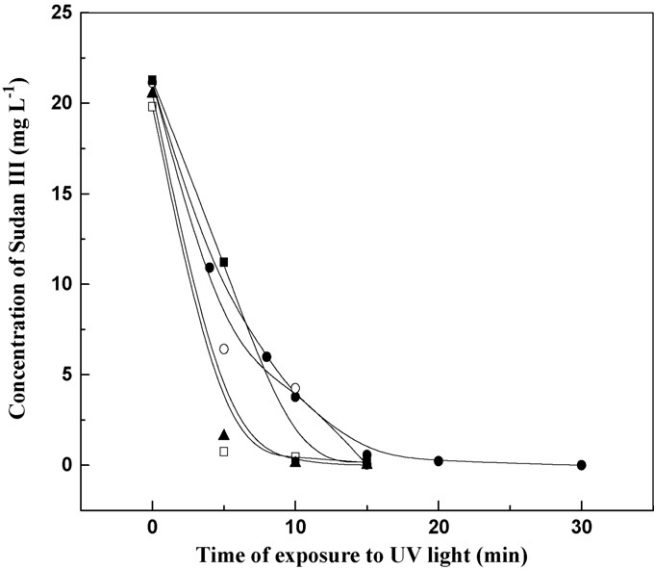

Fig. 5. Effect of solvents on the degradation of Sudan III. ●, ethanol; □, methanol; ◯, 50:50 ethanol:methanol; ▲, 25:75 ethanol:methanol and ■ 75:25 ethanol:methanol.

the surface of TiO_2 gets modified because of the adsorption of cations or anions [18]. The interfacial charge transfer processes depend on the surface characteristics of the TiO_2 particles. The suppression of $OH^{\bullet}$ radicals takes place due to trapping of the conduction band electrons by the adsorbed metal ions.

To investigate the effect of anion, if we compare the reduction in degradation rate by nitrate and chloride at constant copper concentration (200 μM), chloride salt has decreased the rate by 88% whereas the nitrate salt has decreased the rate by 72%. To determine whether this difference was due to different amount of adsorbed Cu^{2+} on the catalyst, the adsorption study of copper on CS TiO_2 was investigated. The solution containing the copper salt was stirred along with the dye and 1 g L^{-1} of the catalyst CS TiO_2 for 30 min. The concentration of Cu^{2+} in the solution after the removal of catalyst particles by centrifugation was determined by the spectrophotometer method using sodium diethyldithiocarbamate. The method of analysis is discussed elsewhere [20]. At 200 μM initial concentration of both chloride and nitrate salt, the amount of adsorbed Cu^{2+} on CS TiO_2 was found to be 19.8 and 22 mg g^{-1} of CS TiO_2, respectively. This indicates that an increased retardation observed in presence of copper chloride compared to that of copper nitrate

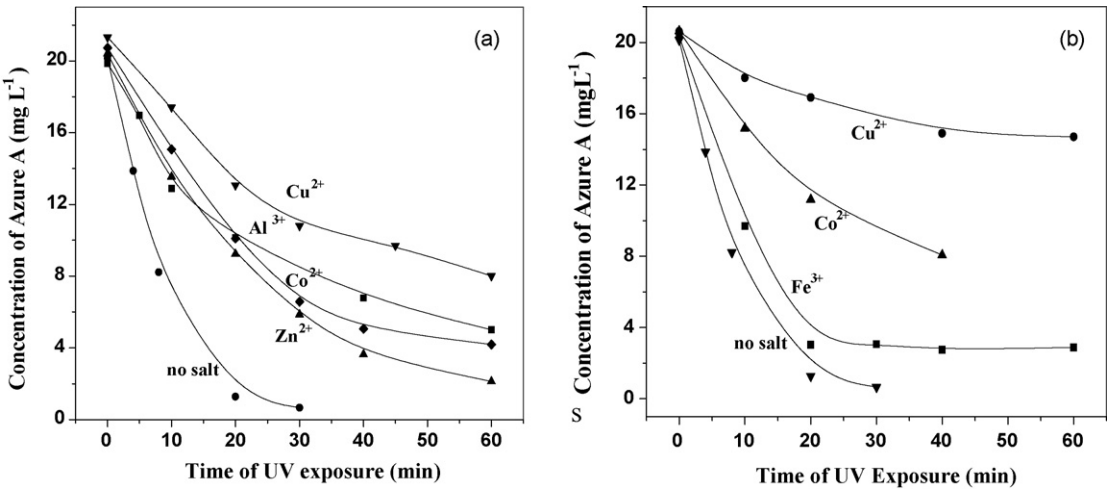

Fig. 6. Effect of (a) different nitrates and (b) different chlorides on the degradation of Azure A.

is not only due to the adsorption on the catalyst. The detrimental effect of chloride ion is probably due to the direct scavenging of $OH^{\bullet}$ by Cl^{-} ions [3,21]. This is in agreement with the results obtained previously [21], where the presence of nitrate and chloride ions had negligible and detrimental effect, respectively, on photocatalytic degradation of ethanol and 2-propanol.

Experiments were conducted at constant initial concentration of the dye Azure A (20 mg L^{-1}) at various initial concentrations of copper nitrate (0–121 mg L^{-1}). Figs. 7 and 8 shows the variation of degradation profile and degradation rate at various concentrations of Cu^{2+}, respectively. The variation of the initial rate of photodegradation of Azure A and the amount of Cu^{2+} adsorbed per unit weight of the catalyst, at various concentration of Cu^{2+} in the solution, is illustrated in the Fig. 8. As the concentration of Cu^{2+} in the solution increases from 0 to 24 mg L^{-1}, the amount of adsorbed Cu^{2+} increases and correspondingly, there is a significant decrease in the initial degradation rate of photocatalysis. This illustrates that the retardation is due to Cu^{2+} ions, which scavenges the electrons required for the formation of hydroxyl radicals.

Fig. 9 illustrates the model fit (given by Eq. (2)) with respect to the experimental data at various [Cu^{2+}]. Based on the experiments in the absence of Cu^{2+}, k_0 and K_2 are obtained. Thus, only K_6 and k_7 are unknowns. By non-linear regression of experimentally obtained $1/r_D$ at various [Cu^{2+}], the values of K_6 and k_7 are determined to be 0.6247 L mg^{-1} and 0.0215 min^{-1}, respectively. k_7, k_0 and $(k_0 - k_7)$ refer to the contribution of hole alone, hole plus electron and electron alone towards degradation. It is interesting to compare the values of $k_0 - k_7$ and k_0, which indicates that the percentage of degradation of Azure A, contributed from $OH^{\bullet}$ generated via electron pathway is 80%. In order to verify this conclusion, non-linear regression of experimental data of Chen et al. [18] corresponding to the degradation of dye sulforhodamine B (SRB) was modeled and is shown in Fig. 9. The

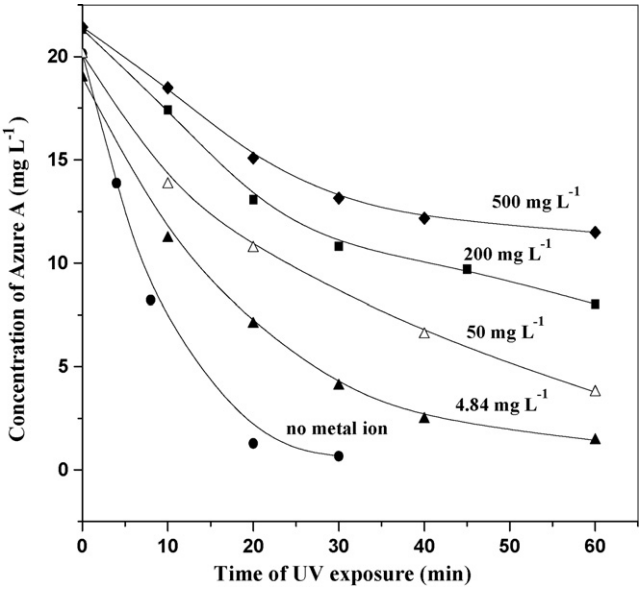

Fig. 7. Concentration profiles of Azure A at various concentrations of Cu^{2+}.

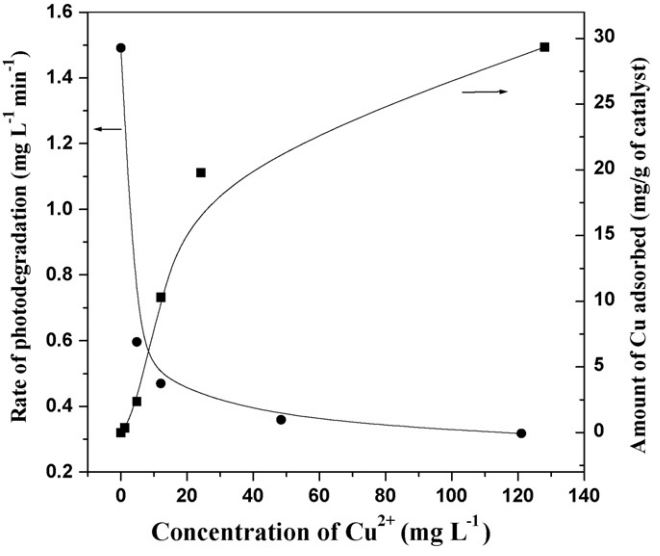

Fig. 8. Variation of degradation rate of Azure A and amount of Cu^{2+} adsorbed at various concentration of Cu^{2+} in solution.

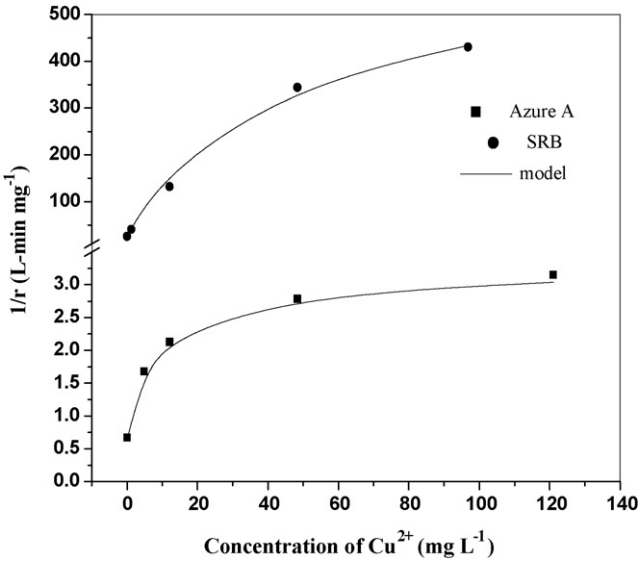

Fig. 9. Variation of inverse of initial rate of degradation with Cu^{2+} concentration for the degradation of Azure A. Model line is based on Eq. (2).

values of k_0 and k_7 are 0.0034 and 0.0001 min^{-1}, respectively. The values of K_2 and K_6 are 0 and 0.67 L mg^{-1}, respectively. In this case, the model shows that the contribution from electron is 95.6%. Also, it indicates that the rate of $OH^{\bullet}$ produced by electrons is much higher than that produced by hole-hydroxyl species interaction and the degradation by direct attack of holes is negligible compared to that obtained by the attack of $OH^{\bullet}$ radicals. Therefore, in the presence of copper, the degradation rate reduces primarily due to a decrease in electron concentration.

The pH effect is often dependent on the nature of the dye [9]. The effect of pH on the photocatalytic degradation of Azure A at an initial concentration of 15 ppm is shown in Fig. 10. The initial rates at both higher and lower pHs, pH 2 and pH 8.2, are twice of the initial rate at neutral pH. At pH of 4, the initial rate is found to be 1.67 times that obtained at the neutral pH. Though it has been reported that the trend of adsorption and photo catalytic degradation would be similar [3], in this case, the adsorption and photodegradation efficiency at various pH are not correlated because the adsorption of the dye does not vary with pH. The parameters that vary with respect to change in pH are concentration of OH radicals, surface charge on the catalyst, ionization state of the substrate, etc. The higher degradation rate at higher pH could be attributed to the higher concentration of OH radicals at higher pH.

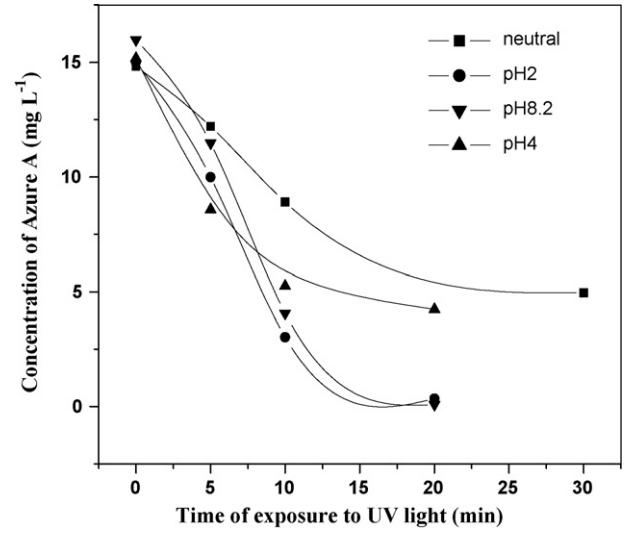

Fig. 10. Concentration profiles of Azure A at various pH.

4. Conclusions

The photocatalytic degradation of Azure (A and B) and Sudan (III and IV) dyes, having similar structure, but different functional groups, were investigated with two catalysts. Among Sudan III and IV, the photocatalytic degradation rates were almost similar. Among Azure A and B, the initial rates were higher for Azure B compared to that of Azure A. The photocatalytic activity of solution combustion synthesized TiO_2 (CS TiO_2) was considerably higher than that of Degussa P-25 for degrading Sudan III and IV. However, in case of Azure A and B, degradation was faster in presence of Degussa P-25 compared to that of CS TiO_2. The effect of solvents and mixed-solvent system on photodegradation of Sudan III was also investigated. The photodegradation rate was found to be higher in solvents with higher polarity. The effect of various metal ions on degradation rate of Azure A was investigated. The retardation effect of metal ions was investigated, both experimentally and modeled using a Langmuir–Hinshelwood kinetic model. The model has proved that the indirect pathway of electrons producing $OH^{\bullet}$ radicals is the main pathway for degradation of the substrate and the direct oxidation of the substrate by holes and the indirect oxidation by holes via $OH^{\bullet}$ radicals has negligible contribution. Thus this model has brought insights into the contribution of holes and electrons towards dye degradation.

Appendix A

$$\text{Electron–hole generation}: \quad TiO_2 \xrightarrow{h\nu} h^+_{VB} + e^- \tag{A.1}$$

$$\text{Recombination}: \quad h^+_{VB} + e^- \xrightarrow{k_r} \text{heat} \tag{A.2}$$

Hydroxyl radical formation:

$$\text{(a) hole pathway}: \quad S - OH^- + h^+_{VB} \underset{k'_{tr}}{\overset{k_{tr}}{\rightleftharpoons}} S - OH^{\bullet} \tag{A.3a}$$

$$S - H_2O + h^+_{VB} \underset{k'_{tr}}{\overset{k_{tr}}{\rightleftharpoons}} S - OH^{\bullet} + H^+ \tag{A.3b}$$

$$\text{(b) electron pathway}: \quad e^- + O_2 \xrightarrow{K_{e1}} O_2{}^{-\bullet} \tag{A.4a}$$

$$O_2{}^{-\bullet} + e^- + 2H^+ \xrightarrow{K_{e2}} H_2O_2 \tag{A.4b}$$

$$2O_2{}^{-\bullet} + 2H^+ \xrightarrow{k_{e3}} O_2 + H_2O_2 \tag{A.4c}$$

$$H_2O_2 + e^- \xrightarrow{K_{e4}} OH^{\bullet} + OH^- \tag{A.4d}$$

Mobile species adsorption:

$$\text{(a) dye}: \quad S + D \underset{k'_D}{\overset{k_D}{\rightleftharpoons}} S-D, \quad K_D = \frac{k_D}{k'_D} \tag{A.5a}$$

$$\text{(b) hydroxyl species}: \quad S + OH^{\bullet} \underset{k'_{OH}}{\overset{k_{OH}}{\rightleftharpoons}} S-OH^{\bullet}, \quad K_{OH} = \frac{k_{OH}}{k'_{OH}} \tag{A.5b}$$

$$\text{(c) } Cu^{2+}: \quad S + C^{2+} \underset{k'_C}{\overset{k_C}{\rightleftharpoons}} S-C^{2+}, \quad K_C = \frac{k_C}{k'_C} \tag{A.5c}$$

$$\text{Reduction of copper}: \quad e^- + C^{2+} \xrightarrow{k_{e5}} C^+ \tag{A.6a}$$

$$e^- + S-C^{2+} \xrightarrow{k_{e6}} S-C^+ \tag{A.6b}$$

It is found in an earlier study, that the reduction of Cu^{2+} to copper metal, Cu^0, is very difficult even under UV radiation [22].

Dye degradation:

(a) Direct holes attack:

$$S-D + h^+_{VB} \xrightarrow{K_{hr,a}} S-D^{0+} \rightarrow \text{end species} \tag{A.7a}$$

$$D + h^+_{VB} \xrightarrow{K_{hr,b}} D^{0+} \rightarrow \text{end species} \tag{A.7b}$$

(b) Hydroxy radicals attack:

$$S-D + S-OH^{\bullet} \xrightarrow{K_{ra}} S + S-D'^0 \rightarrow \text{end species} \tag{A.8a}$$

$$D + S-OH^{\bullet} \xrightarrow{K_{rb}} S + D'^0 \rightarrow \text{end species} \tag{A.8b}$$

$$S-D + OH^{\bullet} \xrightarrow{K_{rc}} S-D'^0 \rightarrow \text{end species} \tag{A.8c}$$

$$D + OH^{\bullet} \xrightarrow{K_{rd}} D'^0 \rightarrow \text{end species} \tag{A.8d}$$

Based on the mechanism, the balance for the total hydroxyl species is

$$\begin{aligned}&\frac{d([OH^{\bullet}] + [S-OH^{\bullet}]}{dt}\\ &= k_{tr}[S-OH^{\bullet}][h^+_{VB}]\\ &- k'_{tr}[S-OH^{\bullet}] + k_{tr}[S-H_2O][h^+_{VB}]\\ &- k'_{tr}[S-OH^{\bullet}][H^+] - k_{ra}[S-D][S-OH^{\bullet}]\\ &- k_{rb}[D][S-OH^{\bullet}] - k_{rc}[S-D][OH^{\bullet}] - k_{rd}[D][OH^{\bullet}]\\ &+ k_{e4}[H_2O_2][e^-]\end{aligned} \tag{A.9}$$

The bracketed term refers to the concentration of the species.

The electron concentration balance is

$$\begin{aligned}\frac{d[e^-]}{dt} &= k_e[S] - k_{rc}[e^-][h^+_{VB}] - k_{e1}[e^-][O_2]\\ &- k_{e2}[e^-][O_2^{-\bullet}][H^+]^2 - k_{e4}[H_2O_2][e^-]\\ &- k_{e5}[e^-][C^{2+}] - k_{e6}[e^-][S-C^{2+}]\end{aligned} \tag{A.10}$$

Similarly we can write balance for the concentration of positive holes, H_2O_2, $O_2{}^{-\bullet}$, H^+ etc.

The rate of disappearance of dye can be written as

$$\begin{aligned}-r_D &= k_{hr,a}[S-D][h^+_{VB}] + k_{hr,b}[D][h^+_{VB}]\\ &+ k_{ra}[S-D][S-OH^{\bullet}] + k_{rb}[D][S-OH^{\bullet}]\\ &+ k_{rc}[S-D][OH^{\bullet}] + k_{rd}[D][OH^{\bullet}]\end{aligned} \tag{A.11}$$

From the adsorption equilibrium, the surface concentration of the hydroxyl radical, dye and copper are given as,

$$[S-OH^{\bullet}] = K_{OH}[S][OH^{\bullet}] \tag{A.12}$$

$$[S-D] = K_D[S][D] \tag{A.13}$$

$$[S-C^{2+}] = K_C[S][C^{2+}] \tag{A.14}$$

By applying the quasi steady-state assumption for the hydroxyl radicals, electrons and holes, we get

$$[OH^{\bullet}] = \frac{k_{tr}\{[S-OH^-] + [S-H_2O]\}[h^+_{VB}] + k_{e4}[H_2O_2][e^-]}{K_{OH}\{k'_{tr}[S]\{1+[H^+]\} + k_{ra}K_D[S][D][S] + k_{rb}[D][S]\} + k_{rc}K_D[S][D] + k_{rd}[D]} \tag{A.15}$$

In the above equation, the species concentrations that vary with time are dye and electron concentration. Since the rate of recombination is faster than any other trapping steps,

$$[e^-] = \frac{k_e[S]}{k_r[h^+_{VB}] + k_{e5}[C^{2+}] + k_{e6}K_c[S][C^{2+}]} \tag{A.16}$$

Since $[h^+_{VB}]$ is invariant, the Eq. (A.11) can be written as

$$-r_D = k_{OH}[D] + k_1[D][OH^{\bullet}] \tag{A.17}$$

where

$$k_{OH} = \{k_{hr,a}K_D[S] + k_{hr,b}\}[h^+_{VB}] \tag{A.17a}$$

$$k_1 = k_{ra}K_DK_{OH}[S]^2 + k_{rb}K_{OH}[S] + k_{rc}K_D[S] + k_{rd} \tag{A.17b}$$

From the Eq. (A.15),

$$[OH^{\bullet}] = \frac{k_3}{1+K_2[D]} + \frac{k_{4,0}[e^-]}{1+K_2[D]} \tag{A.18}$$

$$K_2 = \frac{k_{ra}K_D[S][S] + k_{rb}[S] + k_{rc}K_D[S] + k_{rd}}{K_{OH}k'_{tr}[S]\{1+[H^+]\}} \tag{A.18a}$$

$$k_3 = \frac{k_{tr}\{[S-OH^-] + [S-H_2O]\}[h^+_{VB}]}{K_{OH}k'_{tr}[S]\{1+[H^+]\}} \tag{A.18b}$$

$$k_{4,0} = \frac{k_{e4}[H_2O_2]}{K_{OH}k'_{tr}[S]\{1+[H^+]\}} \tag{A.18c}$$

By substituting (A.18) in (A.17), we get

$$-r_D = k_{OH}[D] + k_1[D]\left(\frac{k_3}{1+K_2[D]} + \frac{k_{4,0}[e^-]}{1+K_2[D]}\right) \tag{A.19}$$

From the Eq. (A.16)

$$[e^-] = \frac{k_5}{1 + K_6[C^{2+}]} \tag{A.20}$$

where k_5 and K_6 are given as

$$k_5 = \frac{k_e[S]}{k_{rc}[h^+_{VB}]} \tag{A.20a}$$

$$K_6 = \frac{k_{e5} + k_{e6}K_c[S]}{k_{rc}[h^+_{VB}]} \tag{A.20b}$$

By substituting (A.20) in (A.19), we get

$$-r_D = k_{OH}[D] + k_1[D]\left(\frac{k_3}{1 + K_2[D]} + \left(\frac{k_4}{1 + K_2[D]}\right) \times \left(\frac{1}{1 + K_6[C^{2+}]}\right)\right) \tag{A.21}$$

where $k_4 = k_{4,0}k_5$.

The Eq. (A.21) gives the relation between the photocatalytic degradation rate and the concentration of dye and the metal.

References

[1] R.W. Matthews, Kinetics of photocatalytic oxidation of organic solutes over titanium dioxide, J. Catal. 111 (1988) 264.

[2] C. Dominguez, J. Garcia, M.A. Pedrez, A. Torres, M.A. Galan, Photocatalytic oxidation of organic pollutants in water, Catal. Today 40 (1998) 85.

[3] B.S. Bhatkande, V.G. Pangarkar, Photocatalytic degradation for environmental applications, J. Chem. Technol. Biotechnol. 77 (2001) 102 (a review).

[4] M.R. Hoffmann, S.T. Martin, W. Choi, D.W. Bahnemann, Environmental applications of semiconductor photocatalysis, Chem. Rev. 95 (1995) 69.

[5] S.T. Martin, H. Herrmann, M.R. Hoffmann, Time resolved microwave conductivity. Part 1 – TiO_2 photoreactivity and size quantization, J. Chem. Soc., Faraday Trans. 90 (1994) 3315.

[6] I.K. Konstantinou, T.A. Albanis, TiO_2-assisted photocatalytic degradation of azo dyes in aqueous solution: kinetic and mechanistic investigations, Appl. Catal. B-Environ. 49 (2004) 1 (A review).

[7] Y. Wang, Solar photocatalytic degradation of eight commercial dyes in TiO_2 suspension, Water Res. 34 (2000) 990.

[8] K. Nagaveni, G. Sivalingam, M.S. Hedge, G. Madras, Solar photocatalytic degradation of dyes: high activity of combustion synthesized nano TiO_2, Appl. Catal. B-Environ. 48 (2004) 83.

[9] G. Sivalingam, K. Nagaveni, M.S. Hegde, G. Madras, Photocatalytic degradation of various dyes by combustion synthesized nano anatase TiO_2, Appl. Catal. B-Environ. 45 (2003) 23.

[10] G. Sivalingam, M.H. Priya, G. Madras, Kinetics of the photodegradation of substituted phenols by solution combustion synthesized TiO_2, Appl. Catal. B-Environ. 51 (2004) 67.

[11] M.H. Priya, G. Madras, Photocatalytic degradation of nitrobenzenes with combustion synthesized nano-TiO_2, J. Photochem. Photobiol. A: Chem. 178 (2006) 1.

[12] M.H. Priya, G. Madras, Kinetics of photocatalytic degradation of phenols with multiple substituent groups, J. Photochem. Photobiol. A: Chem. 179 (2006) 256.

[13] H. Hidaka, Photodegradation of surfactants with TiO_2 semiconductor for environmental waste water treatment, Proc. Indian Acad. Sci. 110 (1998) 215.

[14] O. Legrini, E. Oliveros, A.M. Braun, Photochemical processes for water treatment, Chem. Rev. 93 (1993) 671.

[15] G.A. Epling, C. Lin, Investigation of retardation effects on the titanium dioxide photodegradation system, Chemosphere 46 (2002) 937.

[16] E.B. Azevedo, F.R. Aquino Neto, M. Dezotti, TiO_2-photocatalyzed degradation of phenol in saline media: lumped kinetics, intermediates, and acute toxicity, Appl. Catal. B-Environ. 54 (2004) 165.

[17] Y. Dong, J. Chen, C. Li, H. Zhu, Decoloration of three azo dyes in water by photocatalysis of Fe (III)–oxalate complexes/H_2O_2 in the presence of inorganic salts, Dyes Pigments 73 (2007) 261.

[18] C. Chen, X. Li, W. Ma, J. Zhao, Effect of Transition Metal Ions on the TiO_2-Assisted Photodegradation of Dyes under Visible Irradiation: A Probe for the Interfacial Electron Transfer Process and Reaction Mechanism, J. Phys. Chem. B 106 (2002) 318.

[19] T. Aarthi, G. Madras, Photocatalytic Degradation of Rhodamine Dyes with nano-TiO_2, Ind. Eng. Chem. Res. 46 (2007) 7.

[20] A. Claassen, L. Bastings, The photometric determination of copper by extraction as diethyldithiocarabamate—Interferences and their elimination, Fresenius J. Anal. Chem. 153 (1956) 30.

[21] M. Abdullah, K.C.L. Gary, R.W. Matthews, Effects of common inorganic anions on rates of photocatalytic oxidation of organic carbon over illuminated titanium dioxide, J. Phys. Chem. 94 (1990) 6620.

[22] J.M. Hermann, J. Disdier, J. Pichat, Photoassisted platinum deposition on TiO_2 powder using various platinum complexes, J. Phys. Chem. B 90 (1986) 6028.